

*promoting access to White Rose research papers*



**Universities of Leeds, Sheffield and York**  
**<http://eprints.whiterose.ac.uk/>**

---

This is an author produced version of a paper published in **Geophysical Prospecting**.

White Rose Research Online URL for this paper:

<http://eprints.whiterose.ac.uk/75549/>

---

**Published paper:**

Catt, LML, West, LJ and Clark, RA (2009) *The use of reference models from a priori data to guide 2D inversion of electrical resistivity tomography data*.  
Geophysical Prospecting, 57 (6). 1035 – 1048.

<http://dx.doi.org/10.1111/j.1365-2478.2008.00774.x>

---

The Use of Reference Models from a Priori Data to Guide 2D  
Inversion of Electrical Resistivity Tomography (ERT) Data

Lucy M. L. Catt<sup>1</sup> (e-mail: l.catt@see.leeds.ac.uk)

L. Jared West<sup>1</sup>

Roger A. Clark<sup>1</sup>

1. School of Earth and Environment, University of Leeds, LS2 1JT, U.K.

April 30, 2007

## **Keywords**

Resistivity Inversion

Integrated Geophysics

Near Surface

## Abstract

We report a modelling study to investigate the effects of constraining the inversion of Electrical Resistivity Tomography (ERT) data, from surface arrays, with reference models derived from supplementary resistivity data such as borehole resistivity logs, resistivity cone penetrometry (RCPT), and electromagnetic survey. A synthetic resistivity site model of a highly resistive ( $200\ \Omega\text{m}$ ) sand and gravel lens in a low resistivity ( $30\ \Omega\text{m}$ ) clay till was constructed to test the approach. Synthetic Wenner ERT field data were generated from the synthetic site model and contaminated with fifty sets of Gaussian noise with standard deviation of 2%, and a further fifty sets of Gaussian noise with a standard deviation of 5% of the measurement value. Five structured reference models were constructed incorporating top and basal boundaries of the high resistivity lens, simulating one hit with targeted RCPT, while varying lens width. The noisy ERT data were inverted with 1. an homogenous reference model (blind inversion), and 2. the structured reference models (guided inversion).

The results show that, for blind inversions, the resistivity of a small lens with a resistivity of  $200\ \Omega\text{m}$  will be typically underestimated by about  $100\ \Omega\text{m}$ , which is half its value, in the presence of Gaussian noise; this is a consequence of equivalence. Better reconstructions can be achieved using structured reference models, provided that these are structurally similar to the synthetic site model representing the true geoelectrical structure. More importantly, the reference models and resulting solution models that are close approximations to the actual subsurface structure can be identified without knowledge of the synthetic site model. This is done by comparing the misfits between the solution and reference models, which act as a proxy for the misfit between the solution models and the synthetic model, even when the data are noise-contaminated. Essentially, the approach developed uses the additional (non-ERT) data to identify a limited set of the possible solutions to the blind inversion, which are also compatible with that additional data.

# Contents

Introduction	1
Synthetic Data	4
Blind Inversion	7
Guided Inversion	10
Determining the Best Solution Model	14
Discussion	17
Conclusions	19
Acknowledgements	20
References	21

## Introduction

Electrical Resistivity Tomography (ERT), in both 2D and 3D, is a geophysical tool used in geological, hydrological and geotechnical investigations, though 2D ERT is much more commonly used than 3D ERT. ERT is often used to delineate contaminant plumes and geological boundaries, e.g. Aristodemou and Thomas-Betts (2000); Baines, et al. (2002); Bernstone, et al. (2000); Friedel, et al. (2006); Timms and Acworth (2002). ERT data must be inverted to recover a model of the resistivity of the ground in all but the simplest of cases. The inversion of ERT data is both non-unique and underdetermined. A common approach to ERT inversion is to discretise the model by splitting it into a number of rectangular cells, or regions, and use an  $l_2$  model regularisation, e.g. RES2DINV (Loke 2004). This leads to smooth, minimum structure solutions, with graduated boundaries between areas of differing resistivity.

A number of approaches have been taken to guide the inversion of ERT data to a robust, accurate solution. Different model discretisation schemes have been tried, for example Auken, et al. (2005) treat ERT data as a series of 1D soundings in their 1D laterally constrained inversion (1DLCI). Local 1D forward solutions are found for each sounding. The 1D datasets and models are inverted together, with layer depth and resistivity constraints between adjacent 1D solution models that regularise the inversion. This results in a layered 2D model containing laterally smooth variations in resistivity and layer depth/thickness. Auken and Christiansen (2004) extend this approach in the 2D laterally constrained inversion scheme (2DLCI), in which a 1D model consisting of resistivity/thickness pairs is defined beneath each sounding location. The interface depths at each location are treated as nodes and connected together to form layer boundaries, and the resistivity in each layer between adjacent sounding locations is linearly interpolated. The resulting layered model is interpolated onto a finite difference grid, and a full 2D forward solution is found. As in the 1DLCI, lateral layer depth/resistivity constraints are used to regularise the inversion. These techniques produce good results when lateral resistivity

variations are smooth. However, where lateral resistivity changes are rapid, a full 2D inversion is needed (Auken and Christiansen 2004).

Regularisation of the inversion is used to impose a minimum-structure constraint on the solution. This is typically done by applying an  $l_2$  model regularisation. However, where resistivity boundaries are sharp, the solution will not be a good representation of the subsurface. An alternative approach is to use an  $l_1$  model regularisation. This produces a blocky solution, but regions of the subsurface where resistivity varies smoothly will not be well reconstructed (Ellis and Oldenburg 1994).

*A priori* information can be included in the inversion to try and offset these problems. Paasche and Tronicke (2003) invert ERT data collected over shallow aquifers exhibiting low resistivity contrasts, successfully using structured initial models to guide the inversion towards a good solution. The initial models are simple layered models, with boundaries derived from borehole logs and ground penetrating radar data, and resistivities from preliminary inversions of the ERT data using the apparent resistivity pseudosections as initial models. Cardarelli and Fischanger (2006) demonstrate that for an ERT survey over a tomb, inversion using structured reference models based on *a priori* data produces a good solution model. In this case, the reference model is based on prior knowledge of the typical shape of the type of tomb being surveyed. They conclude that the use of structured reference models is a good way to test the validity of geological/geoelectrical assumptions about the subsurface. In a further example, Pidlisecky, et al. (2006) combine ERT and RCPT to image a saltwater plume. An ERT survey was carried out using the fixed subsurface electrodes as current sources. Potentials were measured at the surface and using a mobile electrode mounted on an RCPT probe that also collected RCPT data. The RCPT data informed the initial model for the inversion of the ERT data. Additional geophysical data can be incorporated by carrying out joint inversion of ERT and these additional data, such as seismic data (Gallardo and Meju 2003).

In this study, we seek to improve the solution model of ERT data with which information such as electromagnetic (EM) ground conductivity data, and resistivity cone penetrometry (RCPT) and/or resistivity borehole logs is associated. We consider the case of detecting sand and gravel bodies in clay-rich till sequences in the U.K. Areas of clay-rich tills are potentially good locations for landfills, as the clay retards groundwater movement and prevents leachate escape. When large sand and gravel bodies are present, they will be detected by borehole and trial-pit led site investigation. Smaller bodies that may be missed by such a site investigation may be connected to underlying aquifers, and act as leachate flow routes. Geophysical surveys can be used to supplement borehole and trial pit data, and detect such bodies. The sand and gravel bodies have higher resistivity than the surrounding clay matrix, making them suitable targets for ERT surveys.

This problem requires an inversion methodology that can be guided to produce solution models that contain both smoothly varying resistivity (in the clay-rich matrix and within the sand and gravel bodies) and sharp resistivity boundaries (at the margins of the sand and gravel bodies) and make use of the RCPT data. We choose inversion of ERT data on a grid of rectangular cells that uses  $l_2$  model regularisation in which the solution model is constrained to a reference model, which can contain sharp boundaries.

One problem with using ERT to detect such features is that the resistivity contrast between the body and the surrounding clay matrix tends to be high, and the body may be thin compared to the depth of investigation of the ERT survey. This introduces the potential for equivalence in the solution models produced by inverting the ERT data. Kilner, et al. (2005) used modelling to investigate the effects of equivalence in ERT surveys over clay-rich tills containing sand and gravel bodies, and showed that in the case of a thin, high resistivity ( $100\ \Omega\text{m}$ ) sand layer in a low resistivity ( $15\ \Omega\text{m}$ ) clay, minimum structure inversion constraints resulted in overestimation of the thickness and underestimation of the resistivity of the layer.

We undertook a modelling study that assesses the potential of using structured reference models based on resistivity log or RCPT data to constrain ERT inversion in this geoelectrical setting, the results of which are presented in this paper. Our starting point was the construction of a synthetic site model representing a sand and gravel lens in a clay-rich till. We then forward-modelled a Wenner ERT survey for this synthetic site and contaminated the resulting synthetic ERT data with Gaussian noise. A range of reference models, consistent with synthetic resistivity log data extracted from the synthetic resistivity site model, were then constructed. We used these reference models to guide the inversion of the noise-contaminated ERT data. By using reference models that contain high-resistivity anomalies of the correct thickness, resistivity and depth, we guided the inversion towards the range of possible solution models with the correct depth and resistivity of anomaly, thus suppressing the effects of equivalence in the inversion.

We show that the best solution model (i.e. that closest to the synthetic site model) can be determined quantitatively from a range of solution models generated using different reference models, without reference to the synthetic site model.

## **Synthetic Data**

The synthetic site model is based on observations from the Holderness coast, East Yorkshire, U.K. The Holderness region is a plain of clay-rich till containing glaciofluvial and glaciolacustrine sand, silt and gravel deposits. The area has some of the best-developed and best-exposed deposits of the Devensian glaciation (Berridge and Patterson 1994; Catt 1991a) and can be considered a suitable analogue for other Devensian till plains in the UK.

The geological model on which the synthetic model is based consists of a sand and gravel lens within an homogenous clay-rich till. The sand and gravel lens and clay-rich till are assigned resistivities of  $200 \Omega\text{m}$  and  $30 \Omega\text{m}$  respectively. These values are based on unpublished 2D ERT

fieldwork carried out on clay-rich tills at various sites in North-Eastern England. The shape of the lens is based on cliff exposures from the Holderness sea cliffs that are presented in Catt (1991b) and Berridge and Patterson (1994) and from the authors' inspection of the coastal exposures on the Holderness coast.

Sand and gravel deposits within clay-rich tills are formed as a consequence of meltout and/or outwash processes laying down coarse deposits at the bed of an active glacier (e.g. Ehlers 1996; Sugden and John 1976). Englacial and subglacial channels can form within a glacier. Water flows through these channels, which are oriented predominantly in the direction of ice flow. These channels are fed by crevasses and seepage from the top of the glacier, and range in size from small tubes to sinuous, branching channels with the same form as stream networks. Depending on the relative strength of the glacier and its substrate (bedrock or till), subglacial channels may erode into the till, forming 'canals', or into the ice, forming 'R-channels', or a combination of both, forming 'tunnels', as shown in Figure 1(a) (Hart 1996). As water flows in these channels, fines are carried in suspension, but coarser clasts are deposited. These coarse sediments are preserved within the lodgement till and retain the shape of the original drainage features in plan view. These relict channels are termed ice-directed features, as they are orientated in sympathy with the direction of ice flow. If such features are not substantially affected by later glaciotectonic processes, they are locally approximately 2D, due to their large extent in the direction of ice flow compared to their comparatively small cross section. This makes them suitable targets for 2D ERT surveys. A typical sand and gravel body is shown in Figure 1(b).

[Figure 1 about here.]

The Wenner array was chosen for the synthetic ERT survey. Zhou and Dahlin (2003) and Dahlin and Zhou (2004) carried out a comprehensive comparison of the noise sensitivity and resolving power of ten common electrode arrays, in which they compared the results of  $l_1$

inversion of synthetic datasets for five different geoelectrical models. Overall, they found that the gradient, pole-dipole, dipole-dipole and Schlumberger arrays produced the best results over the geoelectrical models tested, and that the Wenner and Wenner- $\gamma$  arrays were least susceptible to noise. For the case of a buried relict river channel ( $200 \Omega\text{m}$ ) in clay ( $30 \Omega\text{m}$ ), analogous to the model used in this study, they found that the half-Wenner, pole-dipole and gradient arrays gave the best results, with the Wenner, Schlumberger and midpoint-potential-referred arrays also doing well. The pole-dipole and half-Wenner arrays were discounted due to their requirement for a remote electrode, which is not always practical. Of the remaining arrays, although the gradient array produced the best reconstruction overall, the Wenner and Schlumberger arrays better resolved the base of the channel, due to their superior depth resolution. Given that we constrain depth boundaries in the solution models with RCPT, and that the Wenner array has marginally less sensitivity to noise of the two, the Wenner array was chosen for this modelling study.

The dimensions of the lens are normalised to an electrode spacing of  $n = 1$ , for a 41 electrode Wenner array ERT survey. Horizontally, the centre of the body is at  $20n$  and at a depth of  $6.5n$ , which is the approximate median depth of investigation of the 41 electrode Wenner ERT survey (Barker 1979). The lens has a width of  $6.5n$  and a thickness of  $3.25n$ . The synthetic model is shown in Figure 2.

[Figure 2 about here.]

Forward modelling to obtain synthetic field data is carried out using the University of British Columbia Geophysical Inversion Facility (UBC-GIF) code DCIPF2D (UBC-GIF 2001). The synthetic model is interpolated onto the grid to be used in inversion. Using the same grid for forward modelling and inversion allows direct comparison of the synthetic model and the solution models produced by inversion. The synthetic model is smoothed with a radial running average filter of length  $1.5n$ , as shown in Figure 3(a) (testing on a subset of noise-contaminated

synthetic data showed that this led to slightly faster convergence in inversion without altering the misfit relationships discussed in the section on guided inversion). The grid is constructed with  $0.5n$  wide model blocks and block height starting at  $0.25n$  and increasing with depth, and has 3132 cells. The synthetic dataset contains 260 data points on 13 data levels. The apparent resistivity ( $\rho_a$ ) pseudosection is shown in Figure 3(b).

The synthetic data,  $d_{syn}$ , were then contaminated with Gaussian noise. The noisy synthetic data was generated using

$$d_{nsyn} = d_{syn} + G(p \cdot d_{syn} + cI), \quad (1)$$

which relates the noise-contaminated synthetic 2D ERT data to the uncontaminated data.  $I$  is the identity matrix,  $G$  is a diagonal matrix whose elements are drawn from a Gaussian random distribution with zero mean and unit standard deviation,  $p$  is a constant equal to a small fraction of the noise-free value of each data point, and  $c$  is a small constant that acts as a lower limit to ensure that smaller value data points do not have proportionally lower errors than larger value data points.

Fifty independent manifestations of  $G$  were generated. Using these, fifty noisy data sets were created using  $p = 0.05$  (5% noise datasets), and a further fifty with  $p = 0.02$  (2% noise datasets).  $c = 0.001$  was used in both cases. Synthetic data contaminated with 2% and 5% noise for one manifestation of  $G$  are shown in Figure 3(c) and Figure 3(d).

[Figure 3 about here.]

## Blind Inversion

Commonly, there is little or no *a priori* geoelectrical or structural information associated with ERT data. In such cases, blind inversion is carried out. In order to assess the ‘goodness’ of

solution models produced by inversion with structured reference models, we must first carry out blind inversion. This gives a baseline value of goodness of fit on which we must improve using inversions guided by structured reference models.

Inversion is carried out using the UBC-GIF code DCINV2D (UBC-GIF 2001). The global objective function used in this code is (Oldenburg and Li 1994),

$$\begin{aligned} \Psi = & \int \left[ \alpha_s w_s (m - m^{ref})^2 + \alpha_x w_x \left\{ \frac{\partial (m - m^{ref})}{\partial x} \right\}^2 + \alpha_z w_z \left\{ \frac{\partial (m - m^{ref})}{\partial z} \right\}^2 \right] dA \\ & + \lambda \left[ \sum_{i=1}^D \left( \frac{d_i - d_i^{obs}}{\sigma d_i^{obs}} \right)^2 - \Psi_d^* \right], \end{aligned} \quad (2)$$

where  $D$  is the number of data,  $m$  and  $d_i$  ( $i = 1, \dots, D$ ) are the model and associated data for the current iteration,  $d_i^{obs}$  ( $i = 1, \dots, D$ ) are the observed data,  $\sigma d_i^{obs}$  ( $i = 1, \dots, D$ ) are the standard deviations of the data points,  $\Psi_d^*$  is the target data misfit (with an expected value of  $D$ ), and  $m^{ref}$  is the reference model.  $\lambda$  is a Lagrange multiplier. The user chooses the constraint parameters  $\alpha_s$ ,  $\alpha_x$ , and  $\alpha_z$  to control the closeness of  $m$  to  $m^{ref}$  in terms of the smallness of  $m$  and the flatness of  $m$  in the  $x$  and  $z$  directions respectively. When discretised,  $w_s$ ,  $w_x$  and  $w_z$  weight individual model blocks.

To implement a blind inversion using algorithms such as DCINV2D that require a reference model, the flatness and smallness of the solution model,  $m^{sol}$ , must be similar to a homogenous reference model,  $m^{ref}$ . In this case, it is usual to choose the constraint parameters such that  $(\alpha_x \approx \alpha_z) > \alpha_s$ . For each of the fifty 2% noise datasets and fifty 5% noise datasets, the resistivity of  $m^{ref}$  is the average of the apparent resistivity pseudosection for that dataset. The constraint parameters were  $\alpha_x = \alpha_z = 1$  and  $\alpha_s = 0.01$  in all cases. After testing with different values of target data misfits to ensure the data were neither under- nor over-fitted, target data misfits of  $0.68 D$  for the 2% noise datasets and  $0.64 D$  for the 5% data misfits were chosen.

The fifty solution models for the 2% noise datasets and fifty solution models for the 5% noise datasets produced by the blind inversions were then interpolated onto a regular  $0.25 n \times 0.25 n$  grid and cross-correlated with a template of the high-resistivity anomaly in the original synthetic site model, also interpolated onto the regular grid. For each solution model,  $m^{sol}$ , the offset of the reconstructed anomaly centre from the true lens centre in  $x$  and  $z$  ( $x_{off}$ ,  $z_{off}$ ) and the resistivity offset at the point of maximum correlation,  $\rho_{off}$ , was calculated. The resistivity offset is negative if the resistivity at the point of maximum correlation is less than  $200 \Omega\text{m}$ , the true resistivity at the centre of the high-resistivity anomaly, and positive if it is more than  $200 \Omega\text{m}$ . The average values for  $x_{off}$ ,  $z_{off}$ ,  $\rho_{off}$ , their standard deviations and maximum and minimum values, where appropriate, are given in Table 1.

[Table 1 about here.]

Figure 4(a) shows  $\rho_{off}$  plotted against  $x_{off}$  and  $z_{off}$  for each of the fifty blind inversions of the 2% noise datasets. Figure 4(b) shows the same plot for the fifty blind inversions of the 5% noise datasets.

[Figure 4 about here.]

Figure 4 shows the centres of the reconstructed anomalies clustering about the true location of the lens in the synthetic model. The average  $x$  offset,  $\bar{x}_{off}$ , is approximately  $0 n$  for both set of inversions. This is the expected value, as the synthetic model is symmetric about  $x = 20 n$ . The scatter in  $x_{off}$  is greater for the 5% noise datasets, with the standard deviation  $\sigma x_{off} = 0.67 n$  and maximum  $x$  offset  $x_{off} = 1.75 n$ . This is compared to  $\sigma x_{off} = 0.30 n$  and maximum  $x_{off} = 1.00 n$  for the inversions of the 2% noise datasets. For a 4 m electrode spacing and a 26 m-wide by 13 m thick lens at a depth of 13 m these correspond to a possible maximum lateral mislocation of 4 m and 7 m respectively. The average  $z$  offset,  $\bar{z}_{off}$ , is approximately

zero in both cases, and the scatter in  $z$  is much smaller than in  $x$ . Again, there is greater scatter for the 5% noise datasets, with  $\sigma z_{off} = 0.27n$  compared to  $\sigma z_{off} = 0.14n$  for the inversions of the 2% noise datasets. The resistivity of the lens is greatly underestimated by both sets of inversions; the resistivity offsets are  $\rho_{off} = -113 \pm 40 \Omega\text{m}$  for inversions of the 2% noise datasets and  $\rho_{off} = -109 \pm 20 \Omega\text{m}$  for inversions of the 5% noise datasets (errors quoted are  $\pm$  one standard deviation).

Figure 5 shows a selection of the solution models, which illustrate the effects of noise on the solution models. These blind inversions show that, even when only 2% random Gaussian noise is present, the location of the lens may be incorrectly identified. The resistivity of the lens may be underestimated by over half its value. Of the range of possible equivalent solution models that would all honour the data, the inversion has produced those that have lower resistivity and broader boundaries than the original synthetic site model. The underestimation of the anomaly resistivity and errors in reconstructing its location could lead to interpretation of the lens as a sandy clay instead of a sand and gravel, or of the lens being saturated when it is dry. These problems highlight the need for a way of guiding the inversion to a better solution model.

[Figure 5 about here.]

## Guided Inversion

Consider a hypothetical field survey, in which an electromagnetic (EM) ground conductivity survey is used to estimate the areal extent and strike of an anomalous, linear high-resistivity feature. The synthetic ERT data simulate the results of a 2D ERT line passing across the strike of an anomaly such as the one in this hypothetical survey. Some additional data is collected, that has a high vertical resolution and a small sample volume, such as a geophysical borehole log or resistivity cone penetrometry (RCPT) data. In order to use these data to constrain ERT

inversion, it is assumed that these data are an accurate record of the resistivity variation with depth, i.e. that there are no scaling effects and that they are uncontaminated by noise, and that the resistivity probe has been targeted on and passed through the high resistivity anomaly. In our synthetic site study, these high-resolution data are simulated by extracting one column of the synthetic resistivity model. For simplicity, the synthetic vertical resistivity logs were taken from the centre of the high resistivity anomaly. In a real survey, it should be possible to target resistivity logs using EM ground conductivity survey data.

Reference models were generated as follows. Some arbitrary anomaly widths are chosen; in this case widths of 0.5, 1, and 1.5 times the true anomaly width, in order to create a suite of reference models in which the width of the high resistivity anomaly is over- and under-estimated. In reality, widths would be based on the results of an areal EM ground conductivity survey. The top and base of the high resistivity anomaly are fixed according to the synthetic vertical resistivity logs. The background and anomaly resistivity are also defined by the synthetic vertical resistivity logs. Two different geometries of the high resistivity anomaly to be placed in each reference model were chosen; a block and a lens. The block anomalies were constructed by using the RCPT to fix the top and bottom boundary, with widths set to 0.5, 1, and 1.5 times the true anomaly width. The lens anomalies were constructed by fitting arcs of circles to the anomaly boundaries, as shown in Figure 6.

[Figure 6 about here.]

The reference models were smoothed with a running average filter of length  $1.25n$ , so the inversion would not be forced to try and reconstruct very sharp boundaries, to which  $l_2$  model regularisation is not suited. The five structured reference models  $m_A$  through  $m_E$  are shown in Figures 7(a) through 7(e). The synthetic model  $m^{syn}$  is included in Figure 7(f) for comparison.

[Figure 7 about here.]

Model  $m_A$  contains a lens-shaped anomaly, and is most similar to the synthetic model, being constructed by smoothing the synthetic model. The anomaly in  $m_B$  is also lens-shaped, like the synthetic model, but is wider than the lens in the synthetic model. Models  $m_C$  to  $m_E$  contain block-shaped anomalies. Model  $m_C$  has a block half the width of the lens in the synthetic model. Model  $m_D$  has a block of the same width as the lens in the synthetic model. Model  $m_E$  contains a block 1.5 times the width of the lens in the synthetic model.

When *a priori* information is used to construct the reference model we wish to place more emphasis on fitting the smallness of the reference model than we do in blind inversion, since we have incorporated information about the geoelectrical structure of the ground into the reference model. This means we need to use a different set of constraint parameters than we did for the blind inversions. Using  $\alpha_s = \alpha_x = \alpha_z = 1$  allowed the construction of good  $m^{sol}$  that honoured both the data and the reference model through stable inversions. These constraint parameters were used in all further inversions.

Guided inversions were carried out for both the 2% and 5% noise datasets. The same approach was applied successfully for the 2% and 5% noise datasets; the results for the 5% noise datasets only are presented here in detail (the results of the 2% inversions are summarised in the section on determining the best solution model). The same target data misfits were used for the 2% and 5% noise datasets as were used for the blind inversions.

As for the solution models produced by blind inversion, the  $x$  and  $z$  offsets ( $x_{off}$  and  $z_{off}$ ) of the reconstructed high-resistivity anomalies from the true centre of the lens in the synthetic model were calculated, as was the resistivity offset,  $\rho_{off}$ . The average values for  $x_{off}$ ,  $z_{off}$ ,  $\rho_{off}$ , their standard deviations and maximum and minimum values, where appropriate, are given in Table 2.

[Table 2 about here.]

The  $x$  offset,  $x_{off}$ ,  $z$  offset,  $z_{off}$ , and resistivity offset at the centre of the anomaly,  $\rho_{off}$ , for each set of fifty inversions with each of the five reference models is plotted in Figures 8(a) through 8(e). The blind inversion plot is included in Figure 8(f) for comparison.

[Figure 8 about here.]

Figure 8 shows how the solution models compare to the synthetic model in terms of anomaly location and resistivity in the centre of the anomaly. These figures show that guided inversions with models  $m_A$  to  $m_D$  reduce the scatter in the location of the centre of the reconstructed high-resistivity anomaly compared to the blind inversions. For inversions that use  $m_A$ , the model closest to the synthetic model, and  $m_D$ , which contains the block anomaly of the same width as the lens in the synthetic model, all inversions result in solution models that place the anomaly at the correct depth. Inversions using models  $m_A$  to  $m_D$  do a much better job of reconstructing the resistivity of the anomaly than the blind inversions. This is because reference models of approximately the correct anomaly thickness, depth and resistivity have been used, thus guiding the inversion towards the subset of possible equivalent solution models that have the correct resistivity and thickness. In this way, the effects of equivalence in the inversion process have been reduced. Inversions using reference models  $m_A$ ,  $m_B$  and  $m_D$  produce solution models that best reconstruct the true anomaly resistivity and location. These are models containing the two lens-shaped anomalies and the model containing a block-shaped anomaly that is the same width as the lens in the synthetic model. Inversions using  $m_C$  tend to overestimate the resistivity of the anomaly, but do well at locating the lens. Inversions using model  $m_E$  tend to underestimate the anomaly resistivity and there is a high scatter in the  $x$  offset  $x_{off}$ ; these solution models are comparable to the solution models produced in the blind inversion.

The solution models for one noisy data set with the five reference models is shown in Figure 9.

[Figure 9 about here.]

From observation of the solution models, it can be seen that the guided inversions are not simply reproducing the reference models; the solution models are a function of both the reference models and the ERT data. Inversion with  $m_A$ , the reference model that is closest to the synthetic model, has produced the solution model that is closest to the synthetic model. The solution model produced by inversion with  $m_B$  is also close to the synthetic model. Inversions with the blocky reference models  $m_C$  and  $m_D$  both produce solution models that retain the blocky characteristics of the reference models, but do not reproduce them exactly. In both cases, the resistivity of the lens has been recovered much better than in the case of blind inversion. Solution models produced using  $m_D$  reconstruct the high-resistivity anomaly location and resistivity a little better than those produced using  $m_C$ , as shown by Figure 9. However, observation of the solution models shows that the latter set of solution models reconstruct the shape of the anomaly better than those produced using  $m_D$ . The guided inversion with  $m_E$  has produced a solution model that is the least close to its reference model; the resistivity of the block shaped anomaly in the solution model is about  $100\ \Omega\text{m}$  compared to  $200\ \Omega\text{m}$  in the reference model. This solution model is actually worse than the solution model produced by the blind inversion. The solution attribute plots in Figure 8 agree with these observations.

## Determining the Best Solution Model

We have shown that, in the synthetic case, guided inversion of ERT data using reference models based on complementary resistivity information can produce a solution model that is closer to the synthetic model than that produced by blind inversion. In field surveys, we carry out ERT surveys and geophysical logging precisely because we do not know the synthetic model. We can still generate a range of reference models that are equally valid given the additional resistivity information that has been collected (for example, ground conductivity mapping and vertical resistivity logs) and carry out multiple inversions of the ERT data, but we need a quantitative

measure of the closeness of the solution model to the true geoelectrical structure that does not require prior knowledge of that structure.

From (2), recall that we attempt to minimise the misfit between the reconstructed model,  $m$ , and the reference model,  $m^{ref}$ , (the model misfit) while achieving a specified target data misfit. In the absence of noise, if a reference model is used that is not close to the true geoelectrical structure, we can only reduce the model misfit past a certain level at the expense of increasing the data misfit, and vice versa. If a reference model that is close to the true geoelectrical structure is used, the model misfit can be reduced while keeping the data misfit small. If only the reference model changes for the inversion of a given dataset, then the model misfit between the solution model and the reference model,  $\Psi_m^R$ , can be used as a proxy to the misfit between the solution model and the true geoelectrical structure, which in our study is represented by the synthetic model,  $\Psi_m^T$ .

When dealing with noisy data, the importance placed on fitting the data must be reduced, to avoid over-fitting the noise and adding noise artefacts into the solution model. We need to know if the proxy relationship described in the previous paragraph still holds when the data are contaminated with noise. In order to investigate this, the model misfit between the solution model and the true model,  $\Psi_m^T$ , and the model misfit between the solution model and the reference model,  $\Psi_m^R$ , are calculated for all fifty guided inversions with each of the five reference models of the 5% noise datasets, and the fifty blind inversions of the 5% noise datasets.  $\Psi_m^R$  is plotted against  $\Psi_m^T$ . If the proxy relationship holds, the two misfits should be positively correlated.

The quantitative measure of the misfit needs to take account of the fit between only that part of the model that is well-resolved by the Wenner array, so the solution models were masked off to this area before calculation of the misfit. Various measures of misfit were tested to see which could best identify the best solution models for each of the fifty noisy data sets. The misfit

between the final and true models,  $\Psi_m^T$ , was defined and calculated for all solution models. The average of  $\Psi_m^T$  for all fifty inversions with each reference model,  $\bar{\Psi}_m^T$ , was calculated, and a subset of the models was inspected by eye to see if the correct models had been identified as being ‘best’ (closest to the true model).

The initial form of  $\Psi_m^T$ , designed to take into account the smallness and x- and z-flatness misfits between the solution and synthetic models, was

$$\begin{aligned} \Psi_m^T &= \sum_{j=1}^N \sum_{k=1}^M q_{j,k}^2 \Delta x_{j,k} \Delta z_{j,k} \\ &+ \sum_{j=1}^N \sum_{k=1}^{M-1} \left[ (q_{j,k+1} - q_{j,k})^2 \left( \frac{\Delta z_{j,k}}{\delta x_{j,k}} \right) \right] + \sum_{j=1}^{N-1} \sum_{k=1}^M \left[ (q_{j+1,k} - q_{j,k})^2 \left( \frac{\Delta x_{j,k}}{\delta z_{j,k}} \right) \right], \quad (3) \end{aligned}$$

where the solution and reference models have  $N$  by  $M$  area elements,  $q_{j,k} = (m_{j,k}^{\text{sol}} - m_{j,k}^{\text{syn}})$  ( $j = 1, \dots, N, k = 1, \dots, M$ ),  $\Delta x_{j,k}$  and  $\Delta z_{j,k}$  ( $j = 1, \dots, N, k = 1, \dots, M$ ) are the element widths and heights, and  $\delta x_{j,k}$  ( $j = 1, \dots, N, k = 1, \dots, M-1$ ) and  $\delta z_{j,k}$  ( $j = 1, \dots, N-1, k = 1, \dots, M$ ) are the distances between horizontally and vertically adjacent elements respectively. However, this definition of the misfit did not reliably identify the ‘best’ models. Various additional definitions of misfit were tested. These definitions ranged through  $l_1$  and  $l_2$  misfits, removing the smallness or flatness terms and changing units of  $m$  ( $\log \sigma$ ,  $\sigma$  or  $\rho$ ). The misfit that best identified the best solution models was simply

$$\Psi_m^T = \sum_{j=1}^N \sum_{k=1}^M q_{j,k}^2 \Delta x_{j,k} \Delta z_{j,k} \quad (4)$$

where  $q$  is a conductivity model (in  $\text{mSm}^{-1}$ ).  $\Psi_m^R$  with the same form was then calculated and plotted against  $\Psi_m^T$ , as shown in Figure 10(a). The plot shows a positive correlation, showing that the proxy relationship holds for this form of the misfit for data contaminated with Gaussian noise. The same plot for the 2% noise datasets is shown in Figure 10(b). Again, a positive correlation is observed, though the relationship appears further from linear, especially for the

blind inversions.

[Figure 10 about here.]

Table 3 shows the average misfits  $\bar{\Psi}_m^T$  and  $\bar{\Psi}_m^R$  for each reference model.

[Table 3 about here.]

The misfits are in agreement both with each other and with the visual assessment of the solution models. Guided inversions with  $m_A$ , the reference model closest to the synthetic model, produce the best solution models and the smallest  $\bar{\Psi}_m^T$  and  $\bar{\Psi}_m^R$ . Guided inversions with  $m_E$ , the reference model least similar to the synthetic model, produce solution models that are worse than those produced by blind inversions, and produce greater  $\bar{\Psi}_m^T$  and  $\bar{\Psi}_m^R$  than the blind inversions.

## Discussion

We have shown that when data are contaminated by noise, the solution models produced by blind inversion of these data can mislocate a small, high resistivity anomaly in a conductive matrix, and will severely underestimate the resistivity of that anomaly. Using typical resistivity values for sands and gravels in clay-rich tills, we have quantified the degree to which the anomaly can be mislocated (a 26 m wide by 13 m thick lens at a depth of 13 m may be mislocated by up to 7 m in the presence of 5% Gaussian noise) and to which the resistivity may be underestimated (the resistivity of a 200  $\Omega\text{m}$  anomaly can be underestimated by over 100  $\Omega\text{m}$ ). Inversion of some of the noisy datasets can produce solution models that are very dissimilar to the synthetic model. This demonstrates the need to find some way of improving the solution model.

For noise-free synthetic data, we would expect that the use of a reference model more similar

to the true geoelectrical structure would lead to a better solution model. However, when noise is added to the data, the solution model is a product of the interaction between the inversion algorithm, the data, the reference model and the noise. Previously, we have shown that even when we have ensured that we are not over-constraining the solution model to the reference model, the solution model is better than that produced by blind inversion, even for noisy data. We showed this by comparing the final model to the synthetic (true) model. The inversion has been guided toward the subset of equivalent solution models that contain high-resistivity anomalies of the correct thickness, resistivity and depth.

Real ERT data are collected from sites where we do not know the true geoelectrical structure of the ground (the equivalent of our synthetic model). In this situation, we could construct reference models based on ground conductivity and vertical resistivity log data, as we did for the hypothetical survey in which we carried out guided inversion. All these reference models would be equally valid guesses. Without knowledge of the true geoelectrical structure of the ground, there would be no way of telling which solution model was best. However, we have shown that in such a situation it is possible to determine the best reference model and solution model pair. This is done by calculating the misfit between the solution model and the reference model, which acts as a proxy for the fit between the solution model and the true model, or the geoelectrical structure of the ground.

The next step in our work has been to test the guided inversion approach using field data. Errors in field data are not necessarily Gaussian. The set of equally valid reference models that we would generate from the ground-conductivity and resistivity log data (the *a priori* data) may not be as well constrained as in this synthetic study. More complex deposit geometries may be encountered in the field than the single lens studied here; this may cause the overall misfit over the entire survey area to be large even when it is locally reduced in the region where we possess complementary data. In order to address these issues, a field study has been undertaken at a field site on the East Yorkshire coast, U.K. The field site is well characterised from nearby cliff

exposures, deposit sampling and grain-size analysis and multiple RCPT logs (both electrical and geotechnical). An EM ground conductivity survey was carried out, and multiple 2D ERT lines were collected. In addition to the RCPT logs, these data form a comprehensive geoelectrical dataset. The data were processed according to the approach outlined in this paper. Preliminary results of this field study indicate that this method is successful when used on real data. These results have been presented at international meetings (Catt, et al. 2006).

## Conclusions

In this study, we sought to improve our ability to locate sand and gravel lenses in clay-rich tills using ERT. We approached this problem by looking at the analogous geoelectrical model of a high-resistivity anomaly within a low resistivity matrix. We have shown that it is possible to use guided inversion to achieve solution models that reconstruct the resistivity, shape and depth of such high resistivity anomalies better than is possible with blind inversion. We have shown that it is possible to identify the best solution model from a number of solution models generated using equally valid reference models, even when the data are contaminated with Gaussian noise. The reference models represent guesses of the true geoelectrical structure, being based on *a priori* data from resistivity logs and EM ground conductivity data. We have also shown that it is possible to quality-control the guided inversions by using a proxy relationship identified. This allows us to determine if the solution model produced by the guided inversion is better or worse than that produced by blind inversion. Although this method is based on  $l_2$  regularised inversion, it can be used in areas where we may encounter both smooth and sharp variations in the subsurface, since we can constrain the solution models to a reference model containing smooth or sharp resistivity variations.

The processing flow outlined in this paper has been designed to be applicable to the collection of field data. Preliminary results from a field study in the U.K. have shown this method to be

successful with real data.

## **Acknowledgements**

This research is funded by the Landfill Tax Credit Scheme (LTCS). We thank Keith Mitchell and Mike Haworth of Wardell Armstrong, and Michael Jones of Waste Management Research Ltd. We also thank Professor Tavi Murray of Swansea University for her involvement in the initial stages of this research.

## References

- Aristodemou, E. and Thomas-Betts, A. 2000. DC Resistivity and Induced Polarisation Investigations at a Waste Disposal Site and its Environments. *Journal of Applied Geophysics* **44**(2), 275–302.
- Auken, E. and Christiansen, A. V. 2004. Layered and Laterally Constrained 2D Inversion of Resistivity Data. *Geophysics* **69**(3), 752–761.
- Auken, E., Christiansen, A. V., Jacobsen, B. H., Foged, N., and Sørensen, K. 2005. Piecewise Laterally Constrained Inversion of Resistivity Data. *Geophysical Prospecting* **53**, 497–506.
- Baines, D., Smith, D.G., Froese, D.G., Bauman, P., and Nimeck, G. 2002. Electrical Resistivity Ground Imaging (ERGI): a New Tool for Mapping the Lithology and Geometry of Channel-belts and Valley-fills. *Sedimentology* **49**(3), 441–449.
- Barker, R. D. 1979. Signal Contribution Sections and Their Use in Resistivity Studies. *Geophysical Journal of the Royal Astronomical Society* **59**(1), 123–129.
- Bernstone, C., Dahlin, T., Ohlsson, T., and Hogland, W. 2000. DC-resistivity Mapping of Internal Landfill Structures: Two Pre-excavation Surveys. *Journal of Environmental Geology* **39**(3-4), 360–371.
- Berridge, N. G. and Patterson, J. 1994. *Geology of the Country Around Grimsby and Patrington*. No. 90, 91, 81 and 82 in Geological Society Sheet Memoirs. HMSO, London, first edn. ISBN 0-11-884496-2.
- Cardarelli, E. and Fischanger, F. 2006. 2D Data Modelling by Electrical Resistivity Tomography for Complex Subsurface Geology. *Geophysical Prospecting* **54**, 121–133.
- Catt, J. A. 1991a. Late Devensian Glacial Deposits and Glaciations in Eastern England and the Adjoining Offshore Region. In J. Ehlers, P. L. Gibbard, and J. Rose (eds.). In: *Glacial*

- Deposits in Great Britain and Ireland*, 61–68. A. A. Balkema, Rotterdam. ISBN 90-6191-875-8.
- Catt, J. A. 1991b. The Quaternary History and Glacial Deposits of East Yorkshire. In J. Ehlers, P. L. Gibbard, and J. Rose (eds.). In: *Glacial Deposits in Great Britain and Ireland*, 185–191. A. A. Balkema, Rotterdam. ISBN 90-6191-875-8.
- Catt, L. M. L., West, L. J., and Clark, R. A. 2006. Fusion of Electrical Resistivity Tomography (ERT) and Resistivity Cone Penetrometry (RCPT) Data for Improved Hydrogeophysical Characterisation. In P. J. Binning, P. Engesgaard, H. Dahle, G. F. Pinder, and W. G. Gray (eds.). In: *Proceedings of the XVI International Conference on Computational Methods in Water Resources*.
- Dahlin, T. and Zhou, B. 2004. A Numerical Comparison of 2D Resistivity Imaging with 10 Electrode Arrays. *Geophysical Prospecting* **52**(5), 379–398.
- Ehlers, J. 1996. *Quaternary and Glacial Geology*. Translated by Philip L. Gibbard. John Wiley and Sons, Chichester, first edn.
- Ellis, R. G. and Oldenburg, D. W. 1994. Applied Geophysical Inversion. *Geophysical Journal International* **16**, 5–11.
- Friedel, S., Thielan, A., and Springman, S. M. 2006. Investigation of a Slope Endangered by Rainfall-induced Landslides Using 3D Resistivity Tomography and Geotechnical Testing. *Journal of Applied Geophysics* **60**(2), 100–114.
- Gallardo, L. A. and Meju, M. A. 2003. Characterization of Heterogenous Near-Surface Materials by Joint 2D Inversion of DC Resistivity and Seismic Data. *Geophysical Research Letters* **30**(13), 1–4.
- Hart, J. K. 1996. Subglacial Deformation Associated with a Rigid Bed Environment, Aberdaron, North Wales. *Journal of Glacial Geology and Geomorphology* **RP01**.

- Kilner, M., West, L. J., and Murray, T. 2005. Characterisation of Glacial Sediments using Geophysical Methods for Groundwater Source Protection. *Journal of Applied Geophysics* **57**(2), 33.
- Loke, M. H. 2004. *2D Resistivity & IP Inversion Software; Version 3.54*. Geotomo Software, Penang, Malaysia.
- Oldenburg, D.W. and Li, Y. 1994. Inversion of Induced Polarisation Data. *Geophysics* **59**(2), 1327–1341.
- Paasche, H. and Tronicke, J. 2003. Improving the reliability of electrical imaging by using adapted starting models (P094). EAGE 65th Conference & Exhibition. Four pages.
- Pidlisecky, A., Knight, R., and Haber, E. 2006. Cone-Based Electrical Resistivity Tomography. *Geophysics* **71**(4), G157–G167.
- Sugden, D. E. and John, B. S. 1976. *Glaciers and Landscape*. Edward Arnold. ISBN 0-7131-5840-9.
- Timms, W. and Acworth, R.I. 2002. Origin, Lithology and Weathering Characteristics of Upper Tertiary - Quaternary Clay Aquitard Units on the Lower Murrumbidgee Alluvial Fan. *Australian Journal of Earth Sciences* **49**(3), 525–537.
- UBC-GIF 2001. *A Program Library for Forward Modelling and Inversion of DC Resistivity and Induced Polarization Data Over 2D Structures; Version 3.2*. Developed under the consortium research project Joint/Cooperative Inversion of Geophysical and Geological Data, UBC-Geophysical Inversion Facility, Department of Earth and Ocean Sciences, University of British Columbia, Vancouver, British Columbia.
- Zhou, B. and Dahlin, T. 2003. Properties and Effects of Measurement Errors on 2D Resistivity Imaging Surveying. *Near Surface Geophysics* **1**, 105–117.

## List of Figures

1	(a) Subglacial channel geometries, after Hart (1996), and (b) a typical sand and gravel body exposed in cross-section on the north-east England coast, photographed by R. H. L. Catt (person for scale). The body is outlined by the white, transparent, dashed line. . . . .	26
2	The synthetic model. . . . .	27
3	(a) The synthetic model (the model in Figure 2) interpolated onto the inversion grid and smoothed; (b) the apparent resistivity pseudosection of the synthetic data; (c) the apparent resistivity pseudosection of the synthetic data, contaminated with 2% Gaussian noise and (d) the apparent resistivity pseudosection of the synthetic data contaminated with 5% Gaussian noise. The dots in (b) through (d) are the plotting positions of the individual data points. Note the different resistivity scale in (a). . . . .	28
4	Solution model attributes for (a) the fifty solution models, 2% noise datasets and (b) the fifty solution models, 5% noise datasets; both generated using $\alpha_x = \alpha_z = 1$ , $\alpha_s = 0.01$ . The size of the circle shows the resistivity of the solution model at the point of maximum correlation. The crosses represent a resistivity of $200 \Omega\text{m}$ , the true resistivity of the lens in the synthetic model. The intersection of the dotted lines is the true location of the centre of the lens. Note that where the circles appear filled-in, several reconstructed anomalies have the same offset from the true lens centre but have different resistivities. . . . .	29
5	Some solution models generated by blind inversions (using best-fit homogenous reference models). (a) 2% noise datasets, worst solution model. The resistivity of the lens is underestimated. (b) 2% noise datasets, best solution model. The lens is in the correct location. (c) 5% noise datasets, worst solution model. The resistivity of the lens is underestimated and it is shifted to the sideways and downwards. (d) 5% noise datasets, best solution model. The shape of the lens is distorted, but it placed in the correct location and has the correct resistivity. . . . .	30
6	Construction of the high resistivity anomalies in the reference models. . . . .	31
7	Reference models used in guided inversions. (a) $m_A$ , (b) $m_B$ , (c) $m_C$ , (d) $m_D$ , (e) $m_E$ . (f) The synthetic lens is shown for comparison. . . . .	32

8	Attributes of the solution models produced by inverting the 5% noise datasets with (a) $m_A$ , (b) $m_B$ , (c) $m_C$ , (d) $m_D$ , and (e) $m_E$ with $\alpha_s = \alpha_x = \alpha_z = 1$ . (f) The results of inversion with the homogenous reference model $m_{homog}$ with $\alpha_s = 0.01$ and $\alpha_x = \alpha_z = 1$ are also shown, for comparison. The size of the circle shows the resistivity of the solution model at the point of maximum correlation. The crosses represent a resistivity of $200\Omega\text{m}$ , the true resistivity of the lens in the synthetic model. The intersection of the dotted lines is the true location of the centre of the lens. . . . .	33
9	Solution models after guided inversions of one set of noisy data with (a) $m_A$ , (b) $m_B$ , (c) $m_C$ , (d) $m_D$ , (e) $m_E$ , using $\alpha_s = \alpha_x = \alpha_z = 1$ , and (f) $m_{homog}$ , using $\alpha_s = 0.01$ and $\alpha_x = \alpha_z = 1$ . . . . .	34
10	Misfit of the solution model to the reference model plotted against the misfit of the solution model to the true model for the two hundred and fifty guided inversions and for the fifty blind inversions for both (a) the 5% and (b) the 2% noise data sets. Note the different scales in (a) and (b). . . . .	35

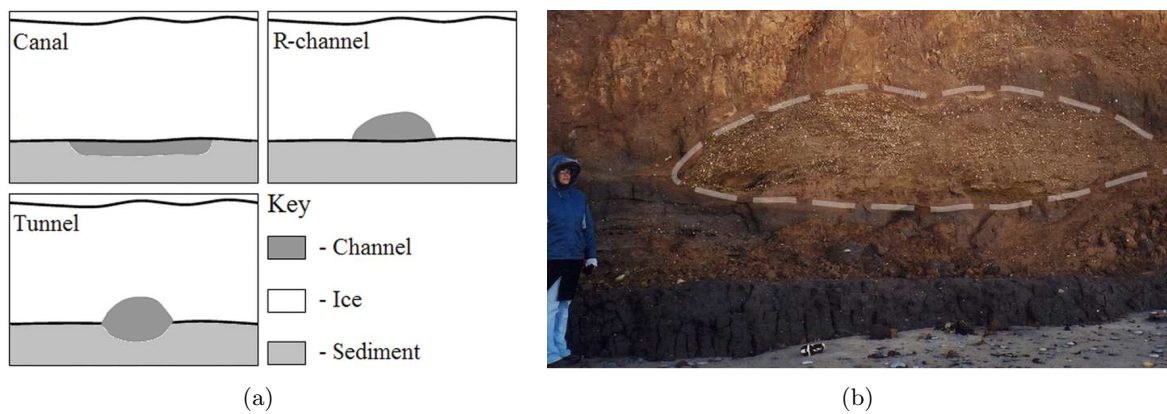


Figure 1: (a) Subglacial channel geometries, after Hart (1996), and (b) a typical sand and gravel body exposed in cross-section on the north-east England coast, photographed by R. H. L. Catt (person for scale). The body is outlined by the white, transparent, dashed line.

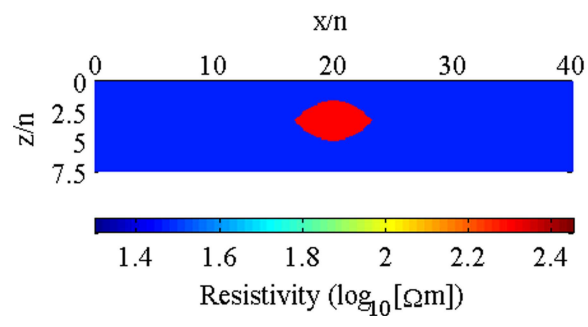


Figure 2: The synthetic model.

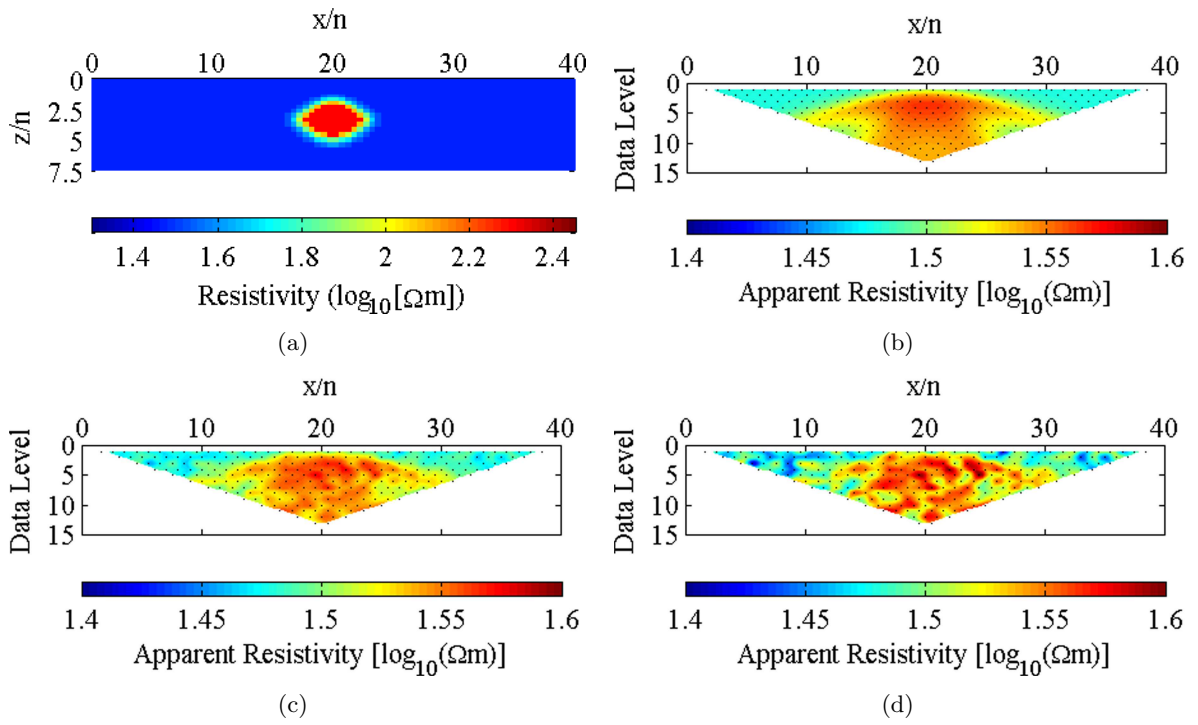


Figure 3: (a) The synthetic model (the model in Figure 2) interpolated onto the inversion grid and smoothed; (b) the apparent resistivity pseudosection of the synthetic data; (c) the apparent resistivity pseudosection of the synthetic data, contaminated with 2% Gaussian noise and (d) the apparent resistivity pseudosection of the synthetic data contaminated with 5% Gaussian noise. The dots in (b) through (d) are the plotting positions of the individual data points. Note the different resistivity scale in (a).

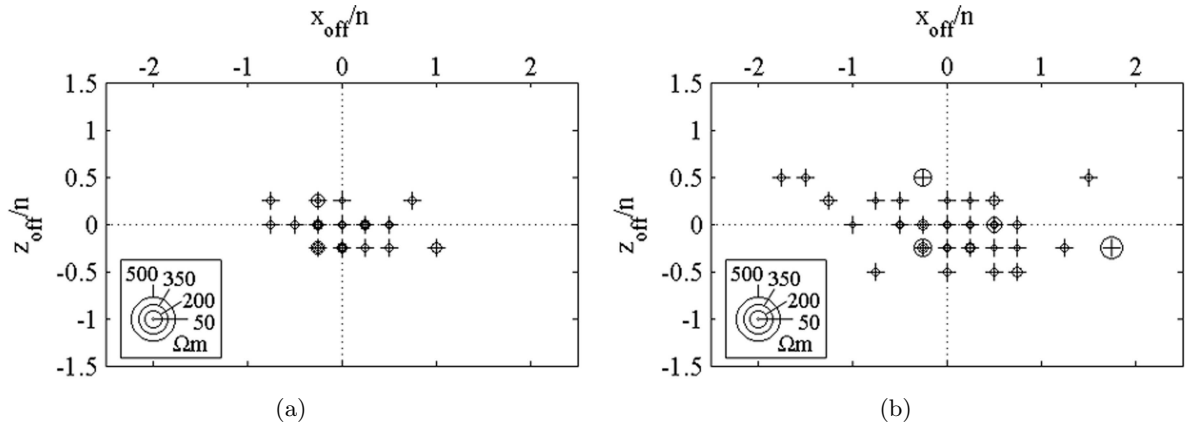


Figure 4: Solution model attributes for (a) the fifty solution models, 2% noise datasets and (b) the fifty solution models, 5% noise datasets; both generated using  $\alpha_x = \alpha_z = 1$ ,  $\alpha_s = 0.01$ . The size of the circle shows the resistivity of the solution model at the point of maximum correlation. The crosses represent a resistivity of  $200 \Omega\text{m}$ , the true resistivity of the lens in the synthetic model. The intersection of the dotted lines is the true location of the centre of the lens. Note that where the circles appear filled-in, several reconstructed anomalies have the same offset from the true lens centre but have different resistivities.

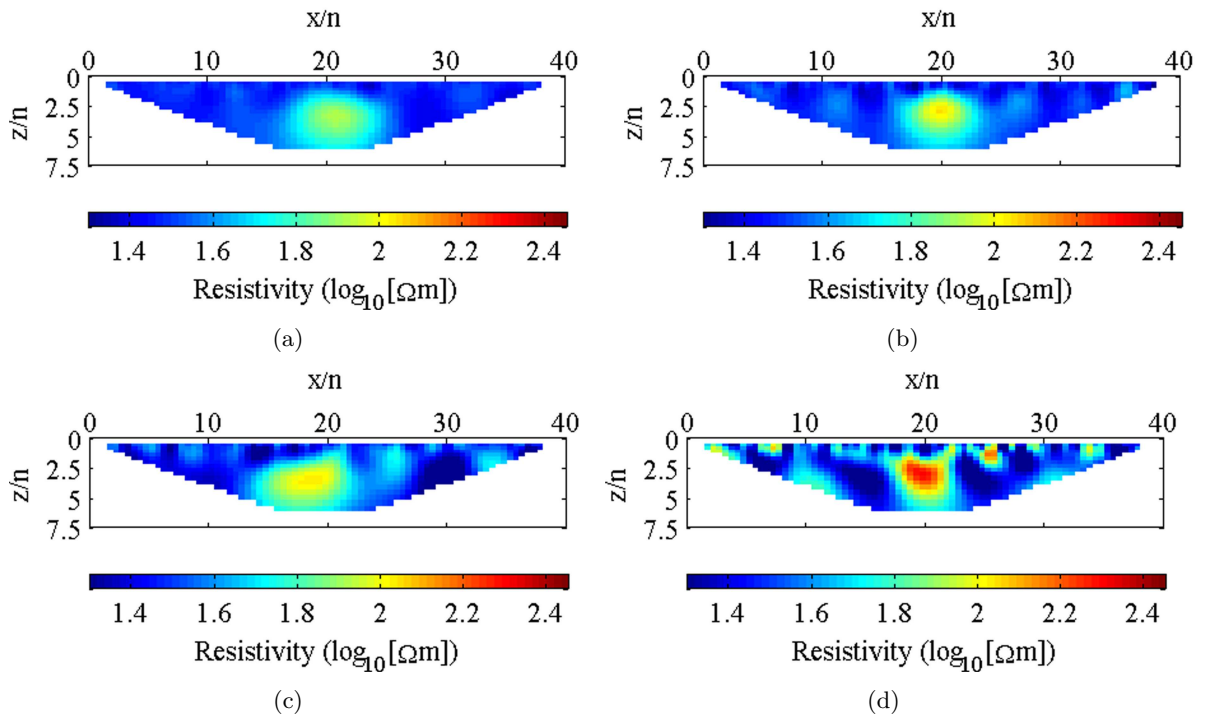


Figure 5: Some solution models generated by blind inversions (using best-fit homogenous reference models). (a) 2% noise datasets, worst solution model. The resistivity of the lens is underestimated. (b) 2% noise datasets, best solution model. The lens is in the correct location. (c) 5% noise datasets, worst solution model. The resistivity of the lens is underestimated and it is shifted to the sideways and downwards. (d) 5% noise datasets, best solution model. The shape of the lens is distorted, but it placed in the correct location and has the correct resistivity.

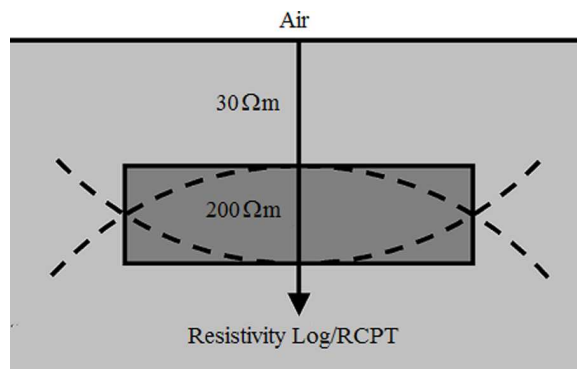


Figure 6: Construction of the high resistivity anomalies in the reference models.

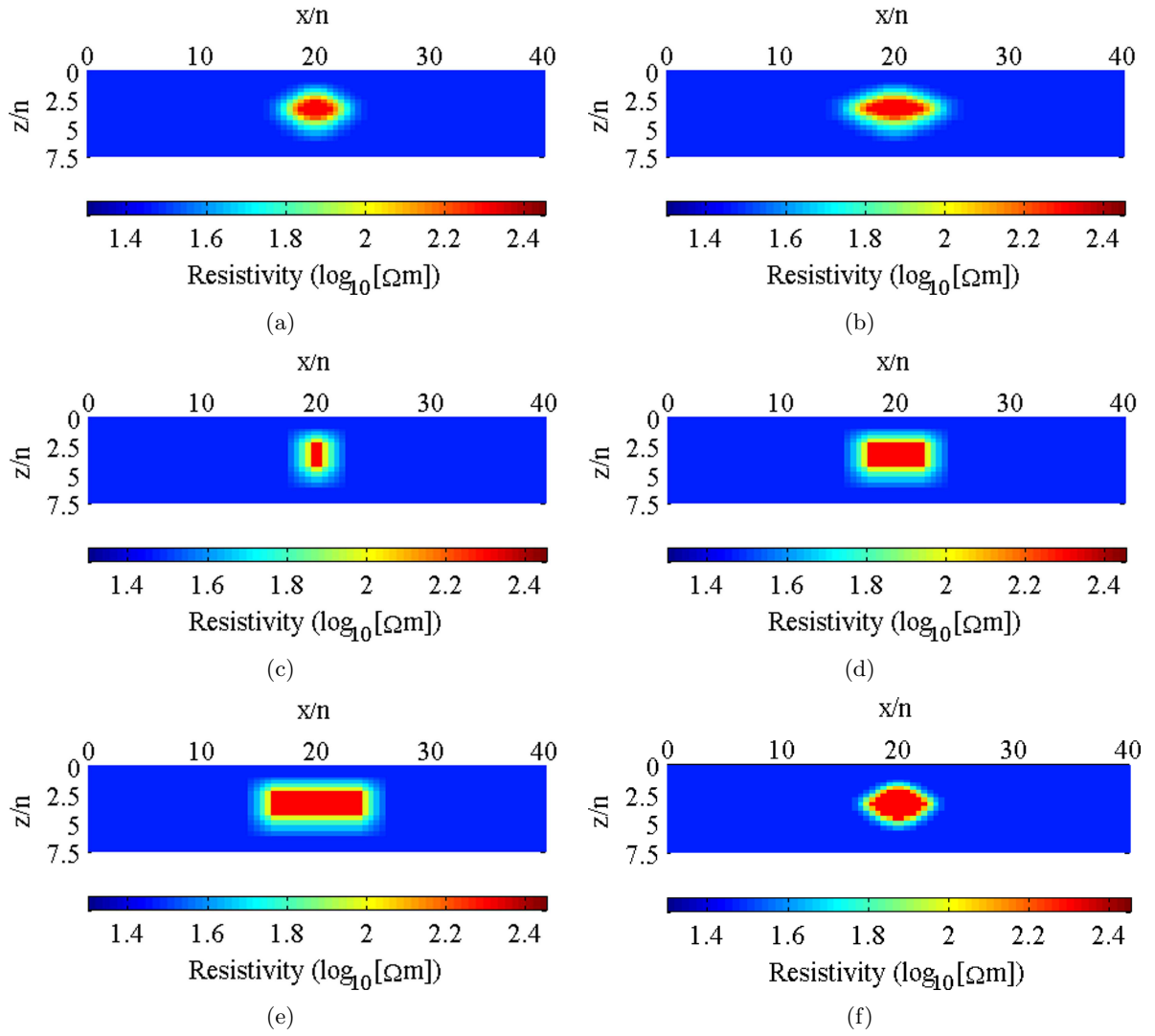


Figure 7: Reference models used in guided inversions. (a)  $m_A$ , (b)  $m_B$ , (c)  $m_C$ , (d)  $m_D$ , (e)  $m_E$ . (f) The synthetic lens is shown for comparison.

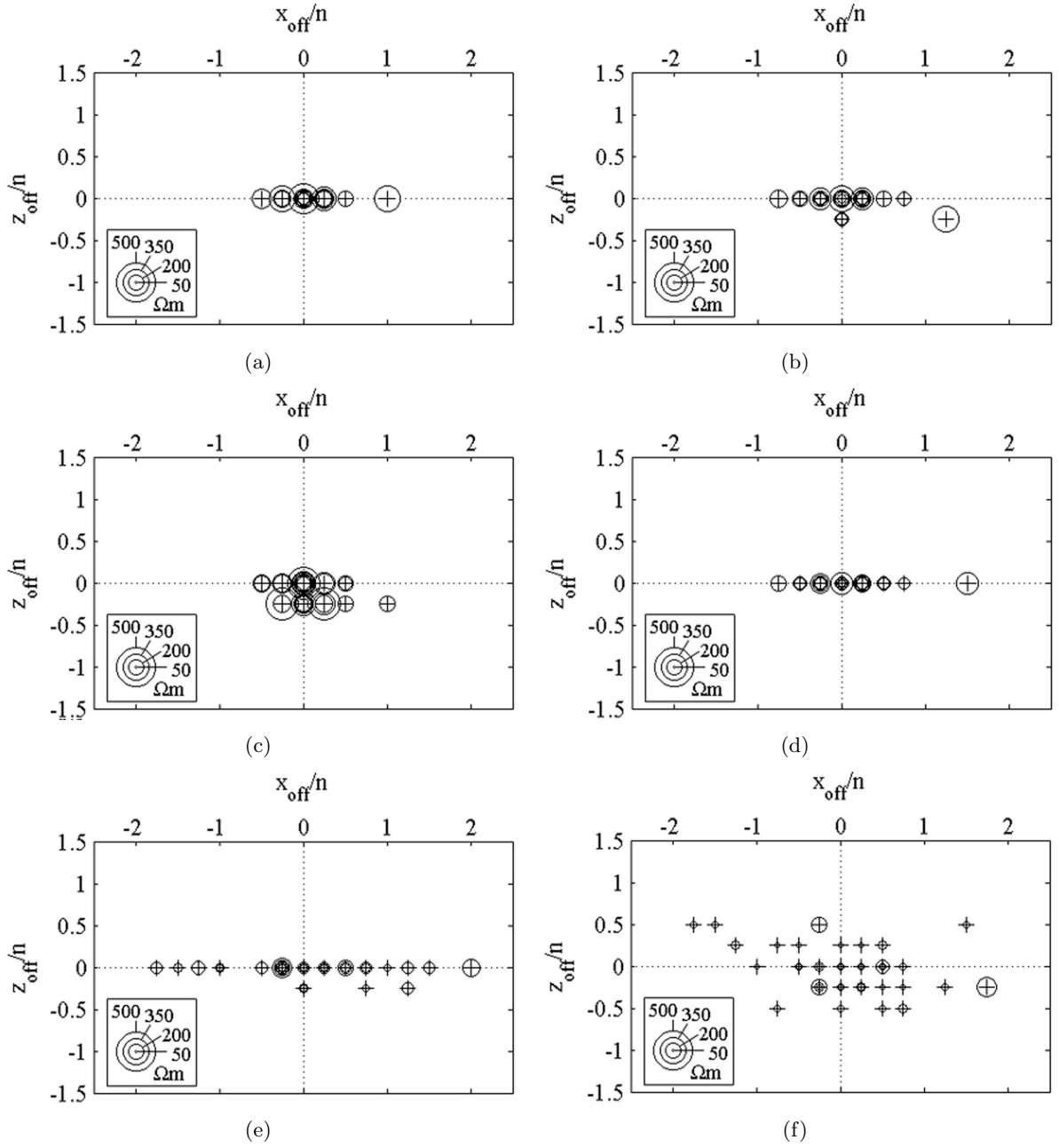


Figure 8: Attributes of the solution models produced by inverting the 5% noise datasets with (a)  $m_A$ , (b)  $m_B$ , (c)  $m_C$ , (d)  $m_D$ , and (e)  $m_E$  with  $\alpha_s = \alpha_x = \alpha_z = 1$ . (f) The results of inversion with the homogenous reference model  $m_{homog}$  with  $\alpha_s = 0.01$  and  $\alpha_x = \alpha_z = 1$  are also shown, for comparison. The size of the circle shows the resistivity of the solution model at the point of maximum correlation. The crosses represent a resistivity of  $200\Omega\text{m}$ , the true resistivity of the lens in the synthetic model. The intersection of the dotted lines is the true location of the centre of the lens.

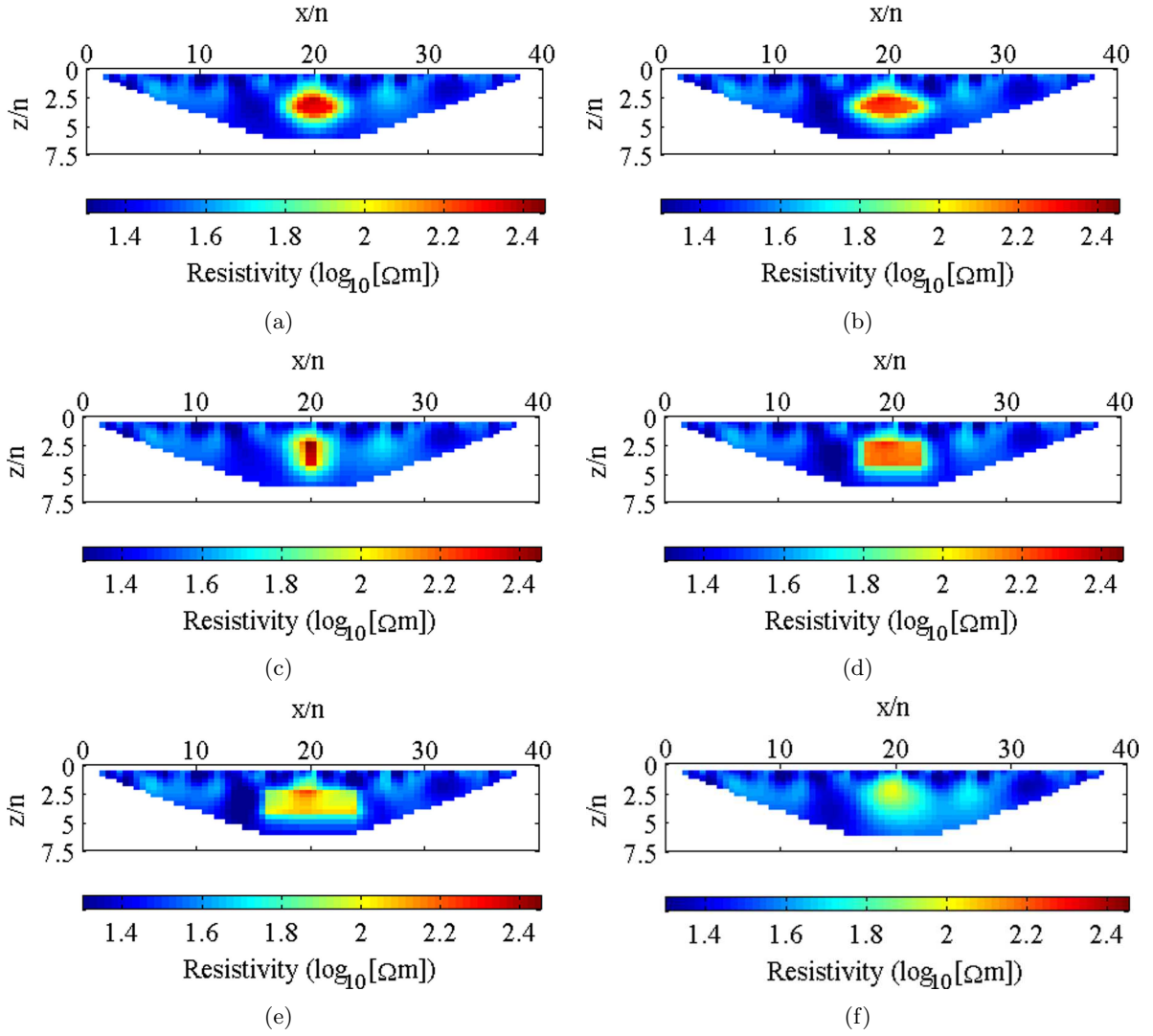


Figure 9: Solution models after guided inversions of one set of noisy data with (a)  $m_A$ , (b)  $m_B$ , (c)  $m_C$ , (d)  $m_D$ , (e)  $m_E$ , using  $\alpha_s = \alpha_x = \alpha_z = 1$ , and (f)  $m_{homog}$ , using  $\alpha_s = 0.01$  and  $\alpha_x = \alpha_z = 1$ .

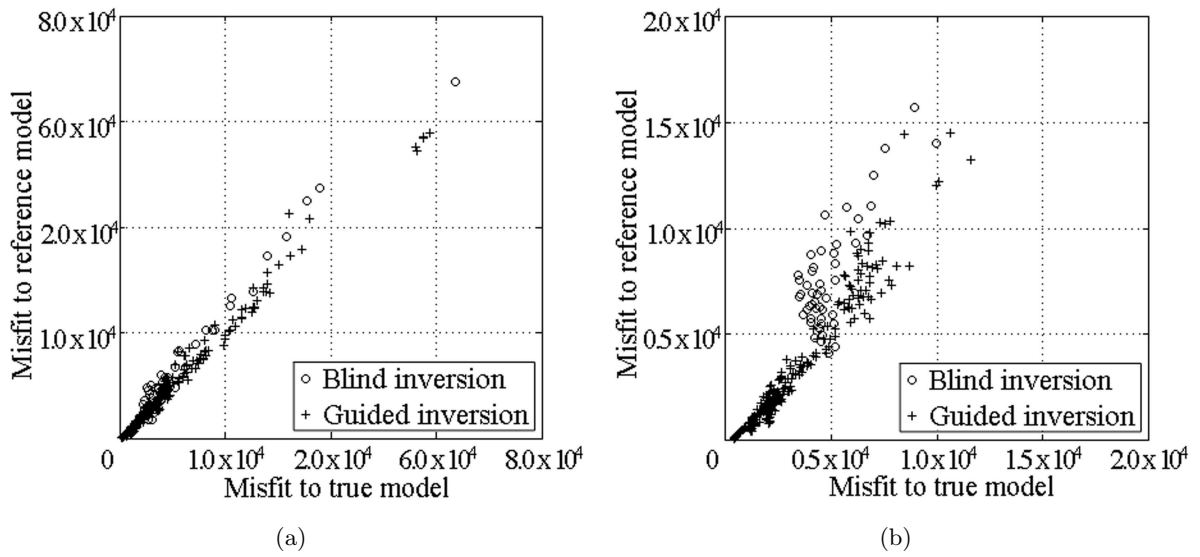


Figure 10: Misfit of the solution model to the reference model plotted against the misfit of the solution model to the true model for the two hundred and fifty guided inversions and for the fifty blind inversions for both (a) the 5% and (b) the 2% noise data sets. Note the different scales in (a) and (b).

## List of Tables

- 1 Final model attributes for the fifty blind inversions of the 2% noise datasets and the fifty blind inversions of the 5% noise datasets, using  $\alpha_s = 0.01$  and  $\alpha_x = \alpha_z = 1$ . 37
- 2 Final model attributes for inversions with 5% noise. The fifty noisy data sets were inverted with reference models  $m_A$  to  $m_E$  with  $\alpha_s = \alpha_x = \alpha_z = 1$ . The results of inversion with the homogenous reference model  $m_{homog}$  with  $\alpha_s = 0.01$  and  $\alpha_x = \alpha_z = 1$  are also shown for comparison. . . . . 38
- 3 Average solution model misfits for guided inversions of all 5% noise datasets with each of the reference models and for the blind inversions. Guided inversions with  $m_A$  to  $m_E$  used  $\alpha_s = \alpha_x = \alpha_z = 1$ . Blind inversion with  $m_{homog}$  used  $\alpha_s = 0.01$  and  $\alpha_x = \alpha_z = 1$ . . . . . 39

	2% noise	5% noise
$x_{off}(n)$	$0.04 \pm 0.33$	$0.02 \pm 0.67$
$x_{off}^{max}(n)$	1.00	1.75
$z_{off}(n)$	$-0.04 \pm 0.14$	$-0.06 \pm 0.27$
$z_{off}^{min}(n)$	-0.25	-0.50
$z_{off}^{max}(n)$	0.25	0.50
$\rho_{off}(\Omega m)$	$-113 \pm 21$	$-109 \pm 40$
$\rho_{off}^{min}(\Omega m)$	-144	-152
$\rho_{off}^{max}(\Omega m)$	-55	48

Table 1: Final model attributes for the fifty blind inversions of the 2% noise datasets and the fifty blind inversions of the 5% noise datasets, using  $\alpha_s = 0.01$  and  $\alpha_x = \alpha_z = 1$ .

	$m_A$	$m_B$	$m_C$	$m_D$	$m_E$	$m_{homog}$
$x_{off} (n)$	$0.03 \pm 0.22$	$0.03 \pm 0.30$	$0.03 \pm 0.25$	$0.03 \pm 0.33$	$0.07 \pm 0.70$	$0.03 \pm 0.67$
$x_{off}^{max} (n)$	1.00	1.25	1.00	1.50	2.00	1.75
$z_{off} (n)$	$0.00 \pm 0.00$	$-0.02 \pm 0.06$	$-0.09 \pm 0.12$	$0.00 \pm 0.00$	$-0.02 \pm 0.07$	$-0.06 \pm 0.27$
$z_{off}^{min} (n)$	0.00	-0.25	-0.25	0.00	-0.25	-0.50
$z_{off}^{max} (n)$	0.00	0.00	0.00	0.00	0.00	0.50
$\rho_{off} (\Omega m)$	$25 \pm 44$	$-7 \pm 41$	$47 \pm 55$	$-32 \pm 35$	$-64 \pm 32$	$-109 \pm 40$
$\rho_{off}^{min} (\Omega m)$	-42	-75	-26	-94	-113	-152
$\rho_{off}^{max} (\Omega m)$	190	140	234	97	48	48

Table 2: Final model attributes for inversions with 5% noise. The fifty noisy data sets were inverted with reference models  $m_A$  to  $m_E$  with  $\alpha_s = \alpha_x = \alpha_z = 1$ . The results of inversion with the homogenous reference model  $m_{homog}$  with  $\alpha_s = 0.01$  and  $\alpha_x = \alpha_z = 1$  are also shown for comparison.

	$m_A$	$m_B$	$m_C$	$m_D$	$m_E$	$m_{homog}$
$\bar{\Psi}_m^T$	7400	8060	8810	8840	13330	12040
$\bar{\Psi}_m^R$	7080	7730	8100	8810	14270	14180

Table 3: Average solution model misfits for guided inversions of all 5% noise datasets with each of the reference models and for the blind inversions. Guided inversions with  $m_A$  to  $m_E$  used  $\alpha_s = \alpha_x = \alpha_z = 1$ . Blind inversion with  $m_{homog}$  used  $\alpha_s = 0.01$  and  $\alpha_x = \alpha_z = 1$ .